Nonlinear Coda Wave Interferometry: Sensitivity to wave-induced material property changes analyzed via numerical simulations in 2D

Guangzhi Chen, Damien Pageot, Odile Abraham, Yuxiang Zhang, Mathieu Chekroun, Vincent Tournat

Ultrasonics 99 (2019) 105968

Contents lists available at ScienceDirect

Ultrasonics

journal homepage: www.elsevier.com/locate/ultras

Nonlinear Coda Wave Interferometry: Sensitivity to wave-induced material property changes analyzed via numerical simulations in 2D

Guangzhi Chen[a,b,c,d,e,*], Damien Pageot[a], Odile Abraham[a], Yuxiang Zhang[b,c,d,e], Mathieu Chekroun[b], Vincent Tournat[b]

[a] IFSTTAR, Dep. GERS, Lab. GeoEND, CS4, F-44344 Bouguenais Cedex, France
[b] Laboratoire d'Acoustique de l'Universitédu Mans, LAUM, UMR 6613 CNRS, Le Mans Université, Avenue Olivier Messiaen, 72085 Le Mans Cedex 9, France
[c] Acoustic Science and Technology Laboratory, Harbin Engineering University, Harbin 150001, China
[d] Key Laboratory of Marine Information Acquisition and Security (Harbin Engineering University), Ministry of Industry and Information Technology, Harbin 150001, China
[e] College of Underwater Acoustic Engineering, Harbin Engineering University, Harbin 150001, China

ARTICLE INFO

Keywords:
Nonlinear Coda Wave Interferometry (NCWI)
Numerical modelling
Effective Damaged Zone (EDZ)
Spectral Element Method (SEM)

ABSTRACT

The numerical studies conducted in this paper are based on our previous research (Chen et al., 2017); through use of the spectral element method, parametric sensitivity studies of Nonlinear Coda Wave Interferometry (NCWI) are established here and divided into two parts. In the first part, CWI observables are found to be proportional to the product of the changes in elastic modulus within the Effective Damaged Zone (EDZ) and the EDZ surface area. The modifications to intrinsic properties are quantified via an overall wave velocity variation, as probed by a reverberated coda wave. However, for high-level changes, CWI may fail due to meaningless decorrelation values. In this context, parametric studies are conducted to yield a maximum range for EDZ contrast and area. To further validate these observations using a more realistic numerical model, instead of introducing a homogeneous EDZ model, the second part of this paper adds random cracks with random orientations into the EDZ of a material sample. The influence of a strong pump wave on localized nonlinear damage is reestablished; results show that the cracks added into the EDZ reduce the property changes required to match the previous experimental dataset.

1. Introduction

In the field of ultrasonic Non-Destructive Testing and Evaluation (NDT&E) of complex materials, e.g. concrete in civil engineering applications and composite materials, existing methods reveal certain limitations, and the need persists to improve the spatial resolution and sensitivity of the diagnosis. A typical way to achieve such improvements in classical ultrasonic methods consists of increasing the frequency, yet in the meantime attenuation also increases due to intrinsic absorption and scattering [2,3] and method limitations are reached. In the scattering process, the amplitudes of direct waves are reduced and a coda wave, i.e. a complex signal composed of multiple scattered contributions, can under certain conditions be observed [4,5]. The coda wave has been shown to be reproducible [6], in containing abundant information on the medium, with very high sensitivity to small disturbances, whether localized or not, of the propagation medium [7–9]. Analyzing coda signals by means of "Coda Wave Interferometry" has often proven to be a powerful technique for monitoring changes in a complex medium [9,10] and imaging or locating defects [11–13]. In parallel, another class of characterization methods, namely nonlinear acoustic methods, has been actively developed for the non-destructive evaluation of complex materials, given their high and selective sensitivity to nonlinear scatterers such as cracks or delamination, i.e. structural defects [14–16]. Interestingly, the elastic nonlinearities originate from internal solid contacts or extremely compliant (relative to the material matrix) elements, e.g. microcracks and interfaces in various types of materials like nonlinear mesoscopic elastic (NME) materials or damaged homogeneous materials [17,18]. Among the range of reported nonlinear acoustic methods, nonlinear modulation has been widely applied to characterize and detect material damage [19,20]. The underlying notion is to excite waves of high amplitude yet relatively low frequency (i.e. pump waves) and then probe the material using a higher-frequency wave. The purpose of the pump wave is to modulate a number of damaged material properties via nonlinear effects.

* Corresponding author.
E-mail address: chenguangzhi@hrbeu.edu.cn (G. Chen).

https://doi.org/10.1016/j.ultras.2019.105968
Received 15 May 2019; Received in revised form 19 July 2019; Accepted 24 July 2019
Available online 26 July 2019
0041-624X/

Afterwards, the probe wave can detect the various pump-induced changes [1,21,22].

Inspired by both these classes of methods, a new set of methods combining nonlinear modulation and Coda Wave Interferometry was proposed by Zhang et al. in 2013 for a cracked glass sample [21]. This so-called nonlinear coda wave interferometry (NCWI) method was then successfully applied to a mortar sample by Hilloulin et al. [9] and subsequently to concrete [10]. In this context, we recently performed a numerical parametric study in [1] using a 2D spectral element method (SEM2D) [23] as a forward modeling tool. In [1], the objective was to reproduce the coda wave signal modifications induced by slight local modifications to the effective elastic properties of a given sample. These modifications were supposedly produced via nonlinear elastic effects from a pump wave of varying amplitude, like in the experiment by Zhang et al. [21] and by considering the same material configuration, *i.e.* a glass sample. For each pump amplitude introduced into the experiment, the associated nonlinear effects were heuristically modeled by slightly varying the elastic properties of an Effective Damaged Zone (EDZ). In practice, such EDZ could help capturing the effects of a given real damage with a reduced number of useful parameters such as the location, size, and level of the damage. These parameters could be useful for the diagnosis or comparison of samples quality, for the evaluation of fatigue. The numerical study [1] thus consisted of a number of linear elastic wave propagation simulations, each extending for a time of hundreds of probe wave periods.

The present paper makes use of the numerical tools developed in [1] to further investigate the impacts of various EDZ parameters on the CWI observables for a multiply reverberated coda wave. The first part tests the method limitations by parametric studies that consider a broad array of elastic EDZ contrasts with the matrix material, for a wide range of relative EDZ sizes. The second part assesses a more realistic numerical model for a cracked zone (replacing the EDZ) and analyzes its effects on the CWI results. Randomly-oriented cracks, in the form of straight segments supporting stress-free boundary conditions, are added in a localized region of the sample. We are able to demonstrate through multiple linear probe wave propagation simulations that the presence of such “simple” cracks can also explain the experimental results of NCWI in cracked glass. Another parametric study is carried out with this configuration, and its results are found to match the previously obtained experimental findings.

2. Dependence of CWI observables on the amount of change in EDZ Young’s modulus and relative area

The Coda Wave Interferometry (CWI) method consists of comparing two signals probing two material states, namely a reference state and a damaged state, as part of a non-destructive evaluation. For this purpose, one recent and powerful tool to estimate the change between these signals is called the *Stretching* method; it evaluates the normalized correlation coefficient $CC(\theta_k)$ between a disturbed signal $u_p(t)$ and a reference signal $u_r(t)$, with the reference signal being stretched in time with the coefficient θ_k ($k = 1, 2, ..., n$ for different levels of stretching). This evaluation corresponds to a global homogeneous increase/decrease in propagation velocity within the medium [24]:

$$CC(\theta_k) = \frac{\int_{t_c-T}^{t_c+T} u_r(t(1+\theta_k))u_p(t)dt}{\sqrt{\int_{t_c-T}^{t_c+T} u_r^2(t(1+\theta_k))dt \int_{t_c-T}^{t_c+T} u_p^2(t)dt}}. \quad (1)$$

The value of the correlation coefficient $CC(\theta_k)$ in Eq. (1) quantitatively represents the similarity of the two signals recorded before and after disturbance of the medium within a selected time window $[t_c - T, t_c + T]$, where t_c is the central time of the window and $2T$ the width of the analyzed window frame. Two CWI observables are traditionally introduced herein, namely: (i) when $CC(\theta_k)$ reaches its maximum value, the relative variation in effective coda velocity is found and written as $\theta = \theta_k = \delta v/v$; and (ii) in order to quantify the level of distortion between the two signals, the remnant decorrelation coefficient *Kd* is introduced as $\mathrm{Kd} = 100(1 - CC(\theta))$.

As reported in [1], in the case without attenuation, the CWI observables (θ and Kd) are found to be proportional to the EDZ contrast for small amounts, i.e. typically property changes of a few %:

$$\theta = \alpha_{\theta}^{E,S}.\left(\frac{\Delta E_{edz}}{E_{mtx}}.S_R\right), \quad (2)$$

$$\mathrm{Kd} = \alpha_{\mathrm{Kd}}^{E,S}.\left(\frac{\Delta E_{edz}}{E_{mtx}}.S_R\right)^2. \quad (3)$$

where $\Delta E_{edz}/E_{mtx}$ corresponds to the changes in Young’s modulus of the EDZ and S_R represents the surface ratio of the EDZ to the total surface. $\alpha_{\theta}^{E,S}$ and $\alpha_{\mathrm{Kd}}^{E,S}$ are the linear coefficients relating the CWI observables to the EDZ contrast. These relations may not remain valid for larger EDZ contrasts or a wider EDZ area. Although the NCWI method is commonly applied to detect a small amount of localized defects, our intention here is to establish the maximum EDZ contrast and area that comply with our reported laws and then analyze their limits.

2.1. Modeling and simulation

The influence of a strong pump wave is not being directly simulated here; instead, it is modeled via Young’s modulus variations over the entire homogeneous EDZ with a given EDZ area ratio. For a determined pump wave amplitude, this approach provides an associated Young’s modulus variation in the EDZ and, as a consequence, an EDZ contrast. A 2D linear elastic simulation of coda wave propagation can then be generated. The square matrix of size 200 mm × 200 mm is assigned as our 2D propagation medium, with a square EDZ located at the matrix center (see Fig. 1a). It was reported earlier that the shape and position of the homogeneous EDZ inside the matrix do not significantly influence the NCWI results [1], mainly because of the reverberating nature of the wave field, when statistically exploring the entire sample according to the same procedure. The parameters and acoustic characteristics of the glass matrix are listed in Table 1.

Similar to our previous study [1], the numerical simulations herein have been run using SEM2D [23], while the propagation medium has been meshed with GMSH [25]. The spatial discretization of the propagation medium has been based on a mesh composed of quadrangular elements capable of reproducing complex geometries (Fig. 1a). The minimum wavelength in the propagation medium is estimated as: $\lambda_{min} \approx 4$ mm. Consequently, when considering the level of precision and cost of numerical calculations, the cell size in this study is set to 6 mm.

To appropriately simulate the application of NCWI to the modeled propagation medium, in theory both pump waves and probe waves are required. As mentioned above, we have elected not to address the complex pump wave influence on the medium and the subsequent nonlinear mixing with the probe wave. The effect of the pump wave is assumed to be displayed by the change in EDZ properties compared to a reference value. The probe wave propagation is simulated starting with the excitation of a windowed chirp signal, at a central frequency of $f_0 = 500$ kHz, a bandwidth of [200 kHz, 800 kHz] (Fig. 1b) and a duration of 0.2 ms. The probe signals are recorded for a duration of 2.5 ms at 12 detection points, equally spaced along the matrix edges.

Although the CWI observables are proven to be only minimally influenced by the source/receiver positions [1], the results presented correspond to the mean value of these parameters over all detection points, in order to further reduce variability. The CWI observables are relative values resulting from a comparison of two states of the sample. In this study, the reference model corresponds to the case of an intact glass sample (Table 1) in both the matrix and the EDZ ($|(\Delta E_{edz}/E_{mtx}).S_R| = 0$). The disturbed state contains the damaged glass

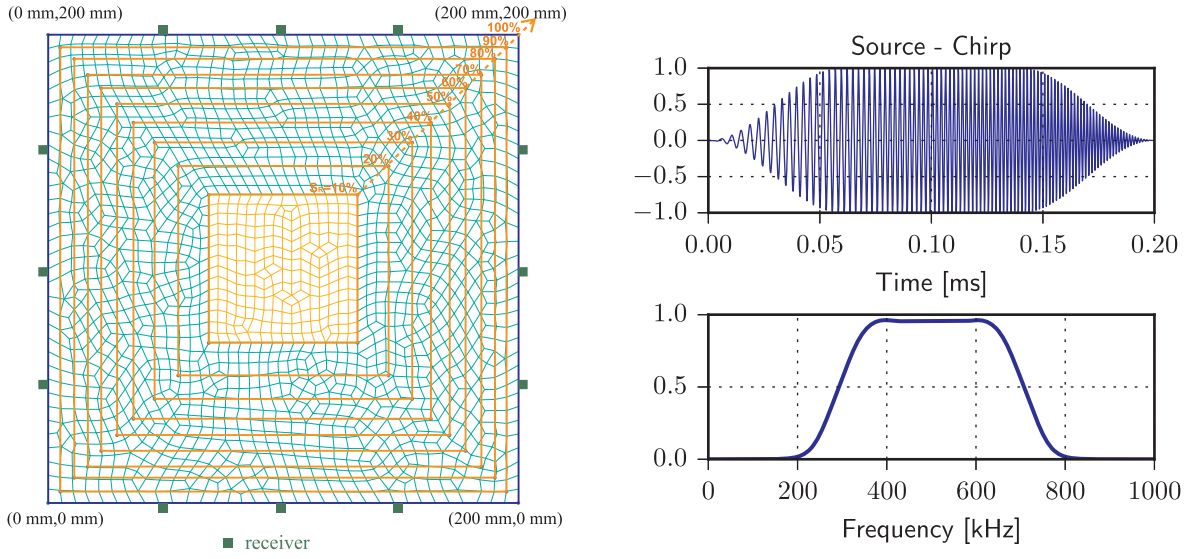

Fig. 1. Numerical configurations: (a) Meshes of the models with ten distinct Effective Damaged Zones (EDZ) of different sizes varying from 10% to 100%; The matrix is marked by the square blue contour and each EDZ is presented by an orange color square. (b) Normalized probe wave source signal: (top) chirp source in the time domain (N.A.); (bottom) normalized amplitude chirp source in the frequency domain.

Table 1
The acoustic caracteristics of the medium on glass.

Glass - properties				
Young's modulus (E) [GPa]	Poisson's ratio (ν)	Mass density (ρ) [Kg·m^{-3}]	P-wave velocity (v_P) [m·s^{-1}]	S-wave velocity (v_S) [m·s^{-1}]
69	0.25	2500	5755	3323

in the EDZ, which has been modeled by changes in Young's modulus within the EDZ ($\Delta E_{edz}/E_{mtx}$). Meanwhile, the matrix outside the EDZ remains unchanged, i.e. intact glass. Note that only negative values of $\Delta E_{edz}/E_{mtx}$ are considered here since softening is universally observed [26,20–22]. Parametric studies have been established with the EDZ contrast change in the case without attenuation, *i.e.* including changes in EDZ area and the corresponding Young's modulus.

We have increased the EDZ surface ratio from 10% to 100% by steps of 10%, with the case of S_R = 100% corresponding to the EDZ filling the entire model area (Fig. 1a). The EDZ material contrast varies up to 3.6×10^{-3} by steps of 0.4×10^{-3}. For the sake of clarity, the EDZ material contrast of 3.6×10^{-3} could be considered as an EDZ area ratio of 10% multiplied by a corresponding Young's modulus change of $\Delta E_{edz}/E_{mtx} = -3.6\%$.

The temporal waveforms shown in Fig. 2 are two examples obtained from samples that were initially identical but damaged under different conditions. The blue lines are the reference signals corresponding to the intact medium ($|(\Delta E_{edz}/E_{mtx})\cdot S_R| = 0$), while the green lines relate to the damaged samples. In the case of Fig. 2a, which results from local damage $|\Delta E_{edz}/E_{mtx}| = 0.40\%$ and $S_R = 10\%$, the EDZ contrast of the damaged medium is: $\Delta E_{edz}/E_{mtx} = 0.4 \times 10^{-3}$. Meanwhile, a higher EDZ contrast of 3.6×10^{-3} stems from the same Young's modulus variation in the EDZ but widespread damage ($|\Delta E_{edz}/E_{mtx}| = 0.4\%$ and $S_R = 90\%$) in the case of Fig. 2b. In the three images from each figure, the signals are illustrated using, from top to bottom, a normal view and two close-up views within an early time window ([0.2, 0.25] ms) and a much later time window ([1.5, 1.55] ms), respectively.

Since the two propagation media are identical when intact, both reference signals (in blue) are also identical. For the very early part of signals (middle images of Fig. 2), regardless of the damage level, no difference can be clearly identified between the signals obtained before and after damage. However, in the late arriving parts of the codas (bottom images), differences in the phase as well as in the amplitude are clearly observed in both figures, confirming the sensitivity of late coda signal contributions due to repetitive probing and multiple scattering in the propagation medium.

2.2. NCWI results

According to the aforementioned process, numerical simulations were performed on 10 models with an EDZ whose surface area ratio S_R was gradually increased from 10% to 100%. In order to obtain 10 identical EDZ contrasts ranging from 0 to 4e-3 for every model, regardless of the S_R value, appropriate changes in Young's modulus were assigned. CWI analyses were then conducted for each model by comparing the corresponding coda signals to the reference signals, i.e. those obtained with a zero EDZ contrast. A time window of [1.5 ms, 2 ms] was selected for the CWI calculation after taking into consideration both method robustness and calculation costs [1]. The CWI results of all 10 models, i.e. θ and Kd respectively, are shown in Fig. 3 a and b.

In most cases, the relations Eq. (2) and Eq. (3) were found to validly describe the CWI result obtained, provided the EDZ contrast remained less than 2.0×10^{-3}. The only exception was the model with S_R = 100%, whose output Kd values remained close to zero for all EDZ contrasts. This result is in line with the theory of Coda Wave Interferometry [24]: since the change in elasticity covers the entire propagation medium, the stretching applied before the Kd calculation accounts for all signal modifications (i.e. a global change of velocity). As the remnant decorrelation coefficient, Kd would then be expected to equal zero. For the other models, once the EDZ contrast exceeds a level of 2.0×10^{-3}, the Kd value stops rising and stabilizes at around 80%, which implies that changes in the propagation medium have caused severe waveform distortion, resulting in coda signals no longer being easily comparable. The CWI results obtained with an EDZ contrast above 2.0×10^{-3} are therefore considered insensitive or saturated and discarded from any further discussion.

On the other hand, it is difficult to ignore the remarkably large gap between the two Kd curves as S_R moves from 90% to 100% (Fig. 3b). In order to understand the meaning behind such an abrupt change in Kd behavior, three more simulations were therefore conducted, using an S_R

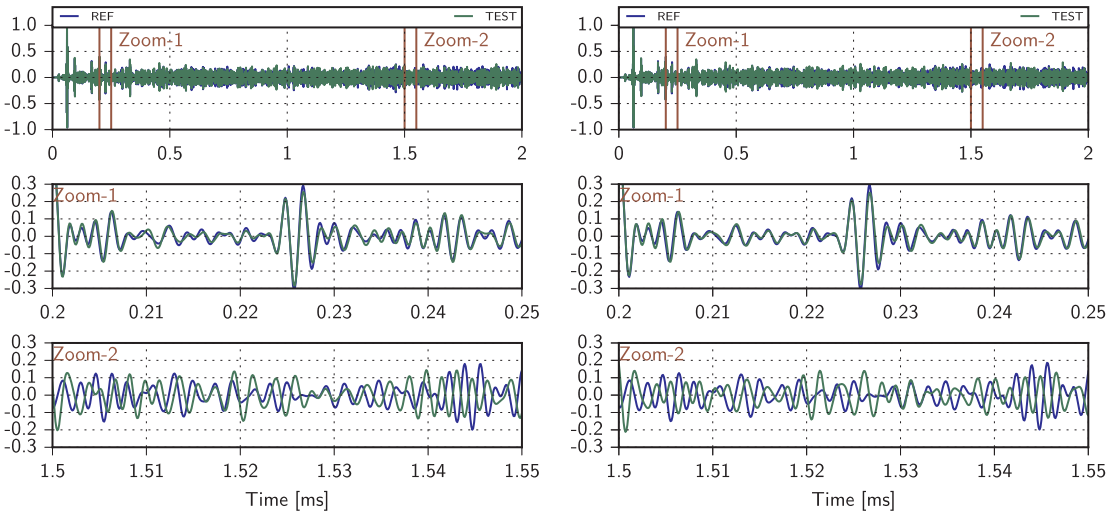

Fig. 2. Examples of temporal signals for two different models different EDZ surface ratio: (a) S_R = 10%; (b) S_R = 90%. The Blue line corresponds to signals from the reference intact material (($\Delta E_{edz}/E_{mtx}$) = 0), while the green line indicates that of damaged material ($\Delta E_{edz}/E_{mtx}$ = −0.4%). (For interpretation of the references to color in this figure legend, the reader is referred to the web version of this article.)

of 92.5%, 95%, and 97.5%. These supplemental CWI results are illustrated in Fig. 4, along with those from models with an S_R of 90% and 100% for purposes of comparison. We observe a fast shift of the Kd curves for these S_R ranges, yet no singular behavior.

With the increased EDZ area, the change in elasticity transitions between a heterogeneous change relative to the reference model to a global change of velocity. This global change is fully captured by the stretching process, leaving no remnant signal distortion and thus yielding a zero Kd. As soon as the elasticity change is heterogeneous, $S_R \neq$ 100%, a remnant decorrelation occurs and Kd becomes nonzero.

This observation suggests that the disturbance to the propagation medium monitored by the CWI, i.e. elasticity reduction in the case of this study, transitions from local to global when S_R lies between 90% and 100%. At S_R = 90%, the corresponding EDZ is of the size 189.74 × 189.74 mm^2, which leaves a lateral bandwidth of undamaged area equal to 5.13 mm.

Based on the theory of acoustic energy equipartition [24], the effective propagation velocity of the coda wave in the studied material (c.f. Table 1) is estimated to be 3,512 m/s, which gives an effective wavelength corresponding to the working frequency band ranging from 4.4 mm to 17.6 mm. This finding suggests that once the distance between the EDZ and the medium boundary becomes comparable or less than the minimum wavelength, the disturbance no longer appears as being local, and the heterogeneity is not well detected. Based on the numerical results obtained, we can conclude that the validity of the relation expressed by Eq. (2) depends solely on the quality of CWI analyses, i.e. Kd values should be less than 80% to compare coda signals.

Yet for the relation described by Eq. (3) to be applicable, two conditions need to be fulfilled: (1) the damage must remain local, i.e. an S_R less than 90%; and (2) the damage level should remain moderate, i.e. an EDZ contrast of less than 2.0 × 10^{-3} in the case considered here (see Table 2).

3. Comparison of numerical results for a homogeneous Effective Damaged Zone (EDZ) model and a microcracked EDZ model

In our previous research [1], the CWI observables between experimental and numerical tests were compared. The influence of the pump wave was modeled by changes in the Young's modulus ($\Delta E_{edz}/E_{mtx}$) and inverse of the quality factors, *i.e.* attenuation coefficient ($\Delta Q_{edz}^{-1}/Q_{mtx}^{-1}$) over a homogeneous EDZ. It was shown that the dependence needed of

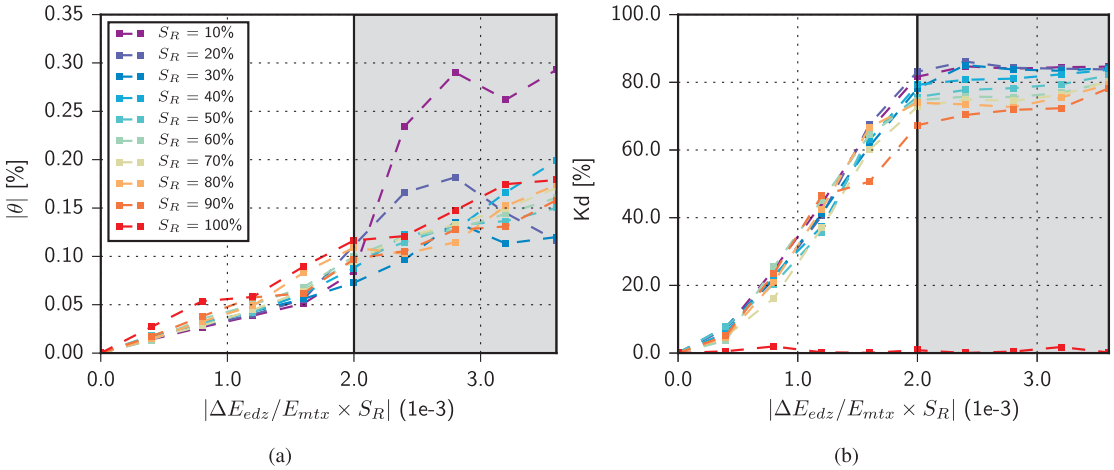

Fig. 3. CWI observables vs. absolute value of EDZ contrast. 10 models are used with different EDZ ratio ranging from 10% to 100% in steps of 10%: (a) Absolute value of relative variation in velocity |θ| vs. $|(\Delta E_{edz}/E_{mtx})\cdot S_R|$; (b) Remnant decorrelation coefficient *Kd* vs. $|(\Delta E_{edz}/E_{mtx})\cdot S_R|$.

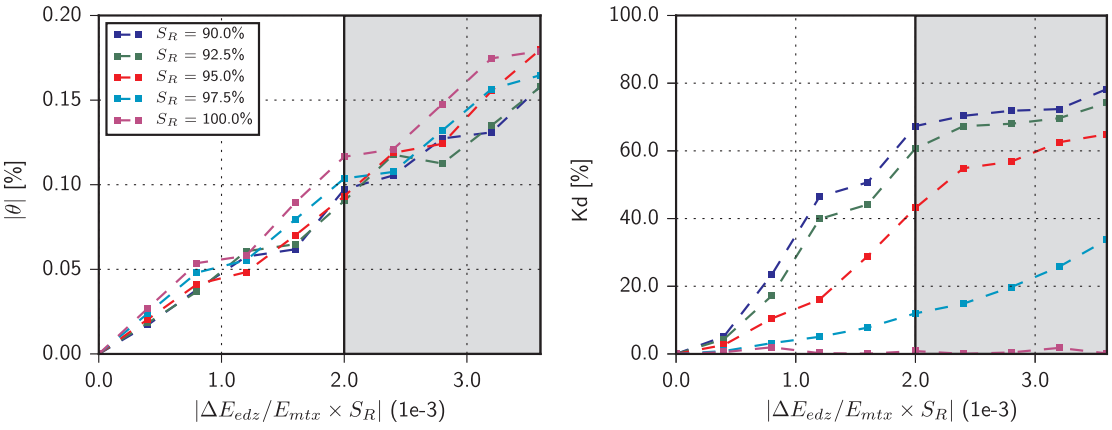

Fig. 4. CWI observables vs. absolute value of EDZ contrast. 5 models are used with different EDZ ratio ranging from 90% to 100% in steps of 2.5%: (a) Absolute value of relative variation in velocity $|\theta|$ vs. $|(\Delta E_{edz}/E_{mtx})\cdot S_R|$; (b) Remnant decorrelation coefficient Kd vs. $|(\Delta E_{edz}/E_{mtx})\cdot S_R|$.

Table 2
EDZ Young's modulus changes and EDZ area ratio corresponding to the maximum EDZ contrast $|(\Delta E_{edz}/E_{mtx})\cdot S_R| = 2.0 \times 10^{-3}$.

Maximum EDZ contrast: $\lvert(\Delta E_{edz}/E_{mtx})\cdot S_R\rvert = 2.0 \times 10^{-3}$			
EDZ aera ratio (S_R)	Maximum change in Young's modulus ($Max.(\Delta E_{edz}/E_{mtx})$)	EDZ aera ratio (S_R)	Maximum change in Young's modulus ($Max.(\Delta E_{edz}/E_{mtx})$)
10%	−2.00%	60%	−0.33%
20%	−1.00%	70%	−0.29%
30%	−0.67%	80%	−0.25%
40%	−0.50%	90%	−0.22%
50%	−0.40%	100%	−0.20%

$\Delta E_{edz}/E_{mtx}$ and $\Delta Q_{edz}^{-1}/Q_{mtx}^{-1}$ in terms of pump amplitude (amplification factor) A_{pump}^{*} is linear. However, the requested quantitative change in attenuation coefficient is unexpectedly high to be matched by the experimental results. In this study, a more realistic numerical model is proposed with cracks of random orientations introduced into the EDZ. Two numerical models, containing a homogeneous or microcracked EDZ, will be compared in the following section.

3.1. Modeling and simulation

The matrix size is set to 200 mm × 200 mm, with a circular EDZ centered at (155 mm, 140 mm); also, 20 cracks are randomly placed inside the EDZ. These cracks are modeled using hollow rhombi with a fixed size of 10 mm × 0.01 mm, in noting that the corresponding aspect ratio (10^3) is in line with that of a crack observed in rock material [27]. Basically therefore, there are lines of stress-free boundary conditions inducing additional wave scattering. As was previously the case, the matrix material is glass (Table 1). For a *standard linear solid* model, over a limited frequency bandwidth, the quality factor could be considered as nearly constant [28,29]. The bulk and shear attenuation, Q_K^{-1} and Q_μ^{-1} are respectively 1,250 and 350 [1].

GMSH is used to mesh the propagation medium, with a cell size set to 6 mm outside the damage zone. The damaged zone itself is meshed with refined meshing cells in order to adapt to the crack size and sharpness (Fig. 5).

The source/receiver configuration is the same as that used in the previous section (Section 2.1), and the reference model corresponds to the case where the material properties are those of intact glass ($\Delta E_{edz}/E_{mtx} = 0$ and $\Delta Q_{edz}^{-1}/Q_{mtx}^{-1} = 0$) in both the matrix and EDZ. The disturbed state corresponds to a damaged glass in the EDZ, which is modeled by $E_{edz} = E_{mtx}(1 + \Delta E_{edz}/E_{mtx})$ and $Q_{edz}^{-1} = Q_{mtx}^{-1}(1 + \Delta Q_{edz}^{-1}/\Delta Q_{mtx}^{-1})$, while the matrix outside the EDZ remains unchanged (i.e. intact glass properties). The parametric studies were re-established with a change in Young's modulus in the EDZ from −0.80% to 0.00%, as well as a change in the attenuation coefficient from 0 to 6.

3.2. NCWI results

By using the model with a microcracked EDZ, the comparisons between numerical results and the experimental findings by Zhang et al. [21] are fully consistent: for each E_{edz} and Q_{edz}^{-1} (or for each pump wave amplitude level in the experiment), a unique pair of values of θ and Kd is obtained. Meaning that in numerical simulations, for given values of θ and Kd obtained for a known A_{pump}, a pair of EDZ properties changes E_{edz} and Q_{edz}^{-1}, could be extracted. The following normalized weighted average $\bar{O}_{CWI}$ [1] is used to compare the estimated experimental values (θ_{exp}, Kd_{exp}) of Zhang et al. [21] with the numerical results (θ, Kd) (Fig. 6). We can observe a clear region of the parameter space maximizing $\bar{O}_{CWI}$ for each pump amplitude tested, thus validating the quantitative agreement between simulations and experiments.

$$\bar{O}_{CWI} = \frac{1}{2}\left\{\left(1 - \frac{|\theta - \theta_{exp}|}{\theta_{exp}}\right) + \left(1 - \frac{|Kd - Kd_{exp}|}{Kd_{exp}}\right)\right\}, \tag{4}$$

Taking the experimental results previously reported in [21] as a reference, the amount of change in intrinsic properties within the EDZ area required for numerical NCWI observations to match experimental ones has been estimated for both models. These results are presented in Fig. 7 and Fig. 8 for purposes of comparison: the blue curve represents results obtained from the model with a homogeneous EDZ, while the green curves depict results from the model with a microcracked EDZ. Thus, for a given pump wave amplitude A_{pump}, the required changes in both Young's modulus $\Delta E_{edz}/E_{mtx}$ and attenuation coefficient $\Delta Q_{edz}^{-1}/Q_{mtx}^{-1}$ are significantly smaller for a microcracked EDZ. For example, for an A_{pump} of 60 dB, the required change in $\Delta Q_{edz}^{-1}/Q_{mtx}^{-1}$ is approx. 57% less for a microcracked EDZ model than for a homogeneous EDZ, which is more reasonable and suggests that the microcracked model provides better agreement with the experimental results. The introduction of microcracks into the EDZ has created more scattering interfaces, and the increase in multiple scattering effects has optimized the numerical model while more closely replicating real experimental conditions.

Since we are not modeling the nonlinear processes occurring at the cracks and simply introducing changes in elasticity and attenuation coefficient in the EDZ, the greater sensitivity obtained for the case with cracks can be explained by the enhanced coda wave sensitivity due to the linear multiple scattering by the cracks. At the given time of the

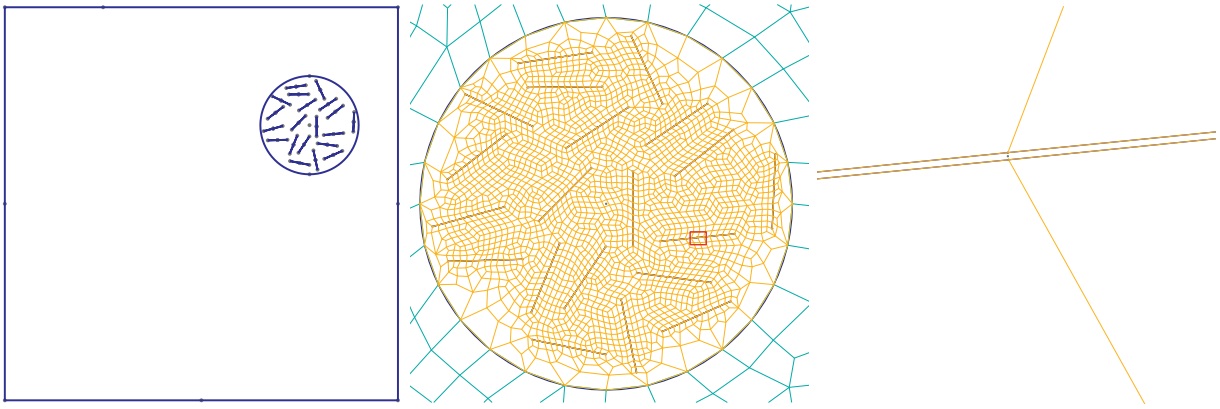

(a) (b) (c)

Fig. 5. Numerical configuration: a homogeneous model with a micro-cracked Effective Damage Zones (EDZ). The size of the crack is mesured 10 mm × 0.01 mm. The blue lines represent the contour of the matrix, the EDZ and the cracks. (a) Numerical model; (b) Zoom of the meshed EDZ; (c) Zoom of one crack corresponding to the red marks in (b). (For interpretation of the references to color in this figure legend, the reader is referred to the web version of this article.)

coda analysis window, the waves have traveled and inspected more of the EDZ when cracks are introduced as additional scatterers than in the case of the simple EDZ, thus explaining the difference in sensitivity. These quantitative results are not only consistent with the findings we reported in Section 2, but also the model configuration is more realistic. The cracking performed in the experimental study [21] is in fact not a controlled process, and the resulting cracks do display a high degree of randomness (shape, size, orientation, etc.). Moreover, it can be expected that for a crack with wavy surfaces [30], the clapping and stick-slip processes generated by pump waves are involved in the nonlinear mixing of coda waves [31,32]. Depending on the pump wave amplitude, some parts of the cracks can stay open, and the presence of cracks generates both linear scattering and nonlinear mixing of coda waves. The cracks we introduced into the numerical model account for the linear scattering process, while the change of EDZ parameters is intended to mimic the nonlinear influence of the pump wave on the medium being probed by the coda wave.

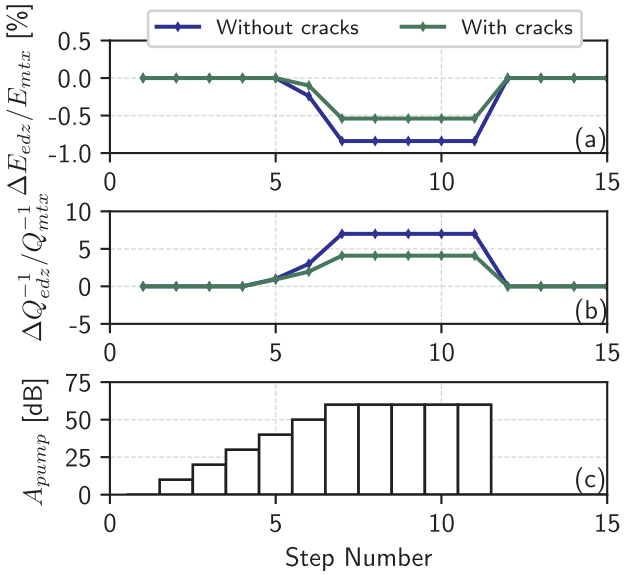

Fig. 7. Property variations in the Effective Damage Zone (EDZ) ($\Delta E_{edz}/E_{mtx}$, $\Delta Q^{-1}_{edz}/Q^{-1}_{mtx}$) compared to the experimental results of Zhang et al. [21] in two case of numerical modelings: (Blue) Previous results of the homogeneous EDZ model; (Green) Numerical results with the micro-cracked EDZ model. (a) $\Delta E_{edz}/E_{mtx}$ vs. step number; (b) $\Delta Q^{-1}_{edz}/Q^{-1}_{mtx}$ vs. step number; and (c) Pump wave excitation amplitude at each step of the test. (For interpretation of the references to color in this figure legend, the reader is referred to the web version of this article.)

4. Conclusion

In this paper, parametric studies of CWI method observables, *i.e.* the relative variation in velocity θ and remnant decorrelation coefficient Kd, have been carried out for a wide range of EDZ contrasts with different EDZ areas. For low levels of localized material damage, the results are shown to be similar to our previous study [1] and consistent with experimental observations [22]. θ is found to be proportional to the EDZ contrast, *i.e.* the change in Young's modulus times the EDZ area ratio $|(\Delta E_{edz}/E_{mtx})\cdot S_R|$, while Kd is found to be quadratically proportional to the EDZ contrast. These two relations have been observed for

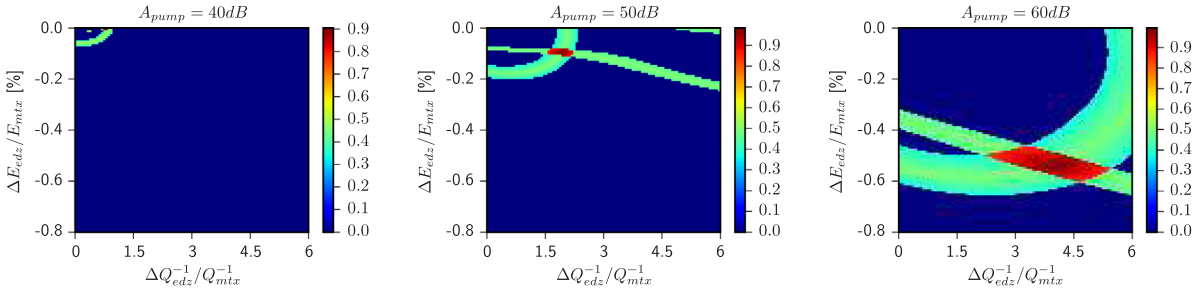

(a) (b) (c)

Fig. 6. Normalized weighted average of the CWI observables values (θ and *Kd*). The coefficients of weighted average for θ and *Kd* are calculated from the group of values θ_{exp} and Kd_{exp} [21] for a given pump wave amplitude: (a) A_{pump} = 40 dB; (b) A_{pump} = 50 dB; (c) A_{pump} = 60 dB.

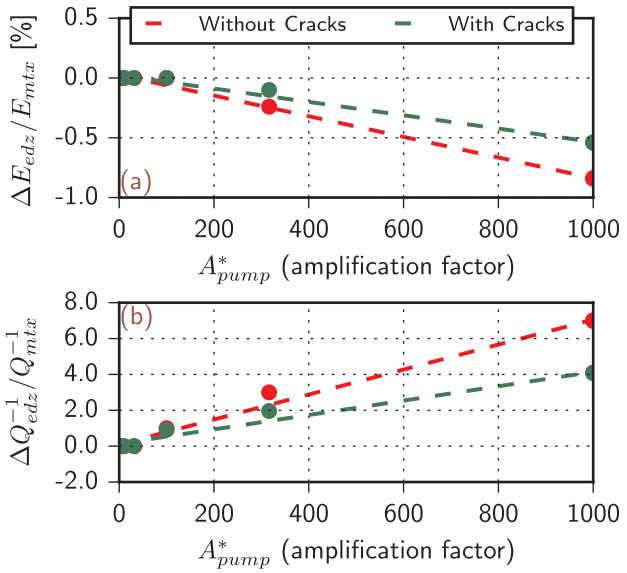

Fig. 8. Property variations in the Effective Damage Zone (EDZ) ($\Delta E_{edz}/E_{mtx}$, $\Delta Q^{-1}_{edz}/Q^{-1}_{mtx}$) vs. pump wave amplitude in the experiment [21] in two case of numerical modelings: (Blue) Previous results of the homogeneous EDZ model; (Green) Numerical results with the micro-cracked EDZ model. (a) $\Delta E_{edz}/E_{mtx}$ vs. normalized pump amplitude; and (b) $\Delta Q^{-1}_{edz}/Q^{-1}_{mtx}$ vs. normalized pump amplitude. Linear fits of the numerical results are proposed. (For interpretation of the references to color in this figure legend, the reader is referred to the web version of this article.)

the EDZ contrast $|(\Delta E_{edz}/E_{mtx})\cdot S_R| \leqslant 2.0 \times 10^{-3}$ when $S_R \leqslant 90\%$. Explanations as to why these relations do not hold outside of these bounds have also been provided. With the introduction of random cracks into the Effective Damaged Zone (EDZ), the identified EDZ material characteristics matching the experimental results derived by Zhang et al. [21] appear to be more realistic, thus enhancing CWI method sensitivity. This numerical simulation study improves the level of understanding of the monitoring and characterization of heterogeneous materials by the CWI method. Moreover, it paves the way to a more quantitative and sensitive use of this method and a possible extension to, for instance, nonlinear imaging.

Acknowledgments

This research was supported by the RFI LMAc Foundation (Recherche Formation Innovation Le Mans Acoustique), set up by France's Loire Valley Regional Council. We are particularly appreciative of Yann Capdeville's valuable work on the numerical method. Our thanks are also extended to Robert Sachs, a native English speaker commissioned to proofread the final draft of this paper.

References

[1] G. Chen, D. Pageot, J.-B. Legland, O. Abraham, M. Chekroun, V. Tournat, Numerical modeling of ultrasonic coda wave interferometry in a multiple scattering medium with a localized nonlinear defect, Wave Motion 72 (2017) 228–243.
[2] D.M. McCann, M.C. Forde, Review of NDT methods in the assessment of concrete and masonry structures, NDT & E Int. 34 (2) (2001) 71–84.
[3] C. Payan, V. Garnier, J. Moysan, P.A. Johnson, Determination of third order elastic constants in a complex solid applying coda wave interferometry, Appl. Phys. Lett. 94 (1) (2009) 011904.
[4] K. Aki, B. Chouet, Origin of coda waves: source, attenuation, and scattering effects, J. Geophys. Res. 80 (23) (1975) 3322–3342.
[5] G. Poupinet, W.L. Ellsworth, J. Fréchet, Monitoring velocity variations in the crust using earthquake doublets: an application to the Calaveras Fault, California, J. Geophys. Res. 89 (1984) 5719–5731.
[6] A. Grêt, R. Snieder, R.C. Aster, P.R. Kyle, Monitoring rapid temporal change in a volcano with coda wave interferometry, Geophys. Res. Lett. 32 (6) (2005) 10–1029.
[7] Y. Zhang, O. Abraham, F. Grondin, A. Loukili, V. Tournat, A.L. Duff, B. Lascoup, O. Durand, Study of stress-induced velocity variation in concrete under direct tensile force and monitoring of the damage level by using thermally-compensated coda wave interferometry, Ultrasonics 52 (8) (2012) 1038–1045.
[8] E. Larose, S. Hall, Monitoring stress related velocity variation in concrete with a 2×10^{-5} relative resolution using diffuse ultrasound, J. Acoust. Soc. Am. 125 (4) (2009) 1853–1856.
[9] B. Hilloulin, Y. Zhang, O. Abraham, A. Loukili, F. Grondin, O. Durand, V. Tournat, Small crack detection in cementitious materials using nonlinear coda wave modulation, NDT & E Int. 68 (2014) 98–104.
[10] J.-B. Legland, Y. Zhang, O. Abraham, O. Durand, V. Tournat, Evaluation of crack status in a meter-size concrete structure using the ultrasonic nonlinear coda wave interferometry, J. Acoust. Soc. Am. 142 (4) (2017) 2233–2241.
[11] E. Larose, A. Obermann, A. Digulescu, T. Planes, J.F. Chaix, F. Mazerolle, G. Moreau, Locating and characterizing a crack in concrete with diffuse ultrasound: a four-point bending test, J. Acoust. Soc. Am. 138 (1) (2015) 232–241.
[12] Y. Zhang, T. Planes, E. Larose, A. Obermann, C. Pospars, G. Moreau, Diffuse ultrasound monitoring of stress and damage development on a 15-ton concrete beam, J. Acoust. Soc. Am. 139 (4) (2016) 1691–1701.
[13] Y. Zhang, E. Larose, L. Moreau, G. d'Ozouville, Three-dimensional in-situ imaging of cracks in concrete using diffuse ultrasound, Struct. Health Monit. 17 (2) (2018) 279–284.
[14] K. Van Den Abeele, P.A. Johnson, A. Sutin, Nonlinear elastic wave spectroscopy (NEWS) techniques to discern material damage, part i: nonlinear wave modulation spectroscopy (NWMS), Res. Nondestr. Eval. 12 (1) (2000) 17–30.
[15] G. Renaud, J. Rivière, P.-Y.L. Bas, P.A. Johnson, Hysteretic nonlinear elasticity of berea sandstone at low-vibrational strain revealed by dynamic acousto-elastic testing, Geophys. Res. Lett. 40 (4) (2013) 715–719.
[16] J.N. Eiras, Q.A. Vu, M. Lott, J. Payá, V. Garnier, C. Payan, Dynamic acousto-elastic test using continuous probe wave and transient vibration to investigate material nonlinearity, Ultrasonics 69 (2016) 29–37.
[17] P.A. Johnson, B. Zinszner, P.N.J. Rasolofosaon, Resonance and elastic nonlinear phenomena in rock, J. Geophys. Res. B: Solid Earth 101 (B5) (1996) 11553–11564.
[18] P.A. Johnson, R.A. Guyer, The astonishing case of mesoscopic elastic nonlinearity, Phys. Today 52 (1999) 30–35.
[19] O. Buck, W.L. Morris, J.M. Richardson, Acoustic harmonic generation at unbonded interfaces and fatigue cracks, Appl. Phys. Lett. 33 (5) (1978) 371–373.
[20] P.A. Johnson, A. Sutin, Slow dynamics and anomalous nonlinear fast dynamics in diverse solids, J. Acoust. Soc. Am. 117 (2005) 124.
[21] Y. Zhang, V. Tournat, O. Abraham, O. Durand, S. Letourneur, A.L. Duff, B. Lascoup, Nonlinear mixing of ultrasonic coda waves with lower frequency-swept pump waves for a global detection of defects in multiple scattering media, J. Appl. Phys. 113 (6) (2013) 064905.
[22] Y. Zhang, V. Tournat, O. Abraham, O. Durand, S. Letourneur, A.L. Duff, B. Lascoup, Nonlinear modulation of ultrasonic coda waves for the global evaluation of damage levels in complex solids, Ultrasonics 73 (2016) 245–252.
[23] D. Komatitsch, J.P. Vilotte, The spectral element method: an effective tool to simulate the seismic response of 2D and 3D geological structures, B. Seismol. Soc. Am. 88 (1998) 5961–5972.
[24] R. Snieder, A. Grêt, H. Douma, J. Scales, Coda wave interferometry for estimating nonlinear behavior in seismic velocity, Science 295 (5563) (2002) 2253–2255.
[25] C. Geuzaine, J.F. Remacle, Gmsh: a three-dimensional finite element mesh generator with built-in pre- and post- processing facilities, Int. J. Numer. Meth. Eng. 79 (11) (2009) 1309–1331.
[26] K.R. Mccall, R. Guyer, Equation of state and wave propagation in hysteretic nonlinear elastic materials, J. Geophys. Res. B: Solid Earth 99 (B12) (1994) 23887–23897.
[27] G.M. Mavko, A. Nur, Effect of non-elliptical cracks on compressibility of rocks, J. Geophys. Res. 83 (9) (1978) 4459–4468.
[28] J.C. Savage, Attenuation of elastic waves in granular mediums, J. Geophys. Res. 70 (1965) 3935–3942.
[29] H.P. Liu, D.L. Anderson, H. Kanamori, Velocity dispersion due to anelasticity; implication for seismology and mantle composition, Geophys. J. Roy. Astr. S. 47 (1976) 41–58.
[30] V.Y. Zaitsev, V.E. Gusev, V.E. Nazarov, B. Castagnède, Interaction of acoustic waves with cracks: elastic and inelastic nonlinearity mechanisms on different time scales, Acoust. Phys. 51 (2005) S67–S77.
[31] P. Blanloeuil, A. Meziane, C. Bacon, 2D finite element modeling of the non-collinear mixing method for detection and characterization of closed cracks, NDT & E Int. 76 (2015) 43–51.
[32] P. Blanloeuil, A. Meziane, A.N. Norris, C. Bacon, Analytical extension of finite element solution for computing the nonlinear far field of ultrasonic waves scattered by a closed crack, Wave Motion 66 (2016) 132–146.